ELSEVIER

Powder Technology 131 (2003) 93–98

POWDER TECHNOLOGY

www.elsevier.com/locate/powtec

A multifractal comminution approach for drilling scaling laws

Alberto Carpinteri*, Nicola Pugno[1]

Department of Structural Engineering and Geotechnics, Politecnico di Torino, Corso Duca degli Abruzzi 24, Turin 10129, Italy

Received 1 June 2002; received in revised form 1 October 2002; accepted 21 November 2002

Abstract

The drilling comminution is theoretically and experimentally analyzed by a multifractal approach. A generalization of the three classical comminution laws [Rittinger, P.R., 1867. Lehrbuch der Aufbereitungskunde. Berlin; Kick, F., 1885. Das Gesetz der Proportionalen Widerstände. Leipzig; Bond F.C., Min. Eng. 193 (1952) 484] has been performed to evaluate the energy dissipation in the process and to compute the mass distribution of the particles. A transitional fractal exponent of the fragment size distribution is experimentally demonstrated to exist. As a consequence, a multifractal scaling law for the partial mass of fragments and its physical interpretation is consistently proposed.

In addition, we show, both theoretically and experimentally, that the drilling strength is strongly size-dependent and cannot be considered a material constant, as classically supposed. Consequently, a multifractal scaling law for the drilling strength is also proposed.

Keywords: Multifractal comminution approach; Drilling scaling laws; Drilling strength

1. Introduction

Fractals are self-similar objects [4,5]. Such scale-invariant systems offer new opportunities for modelling the propagation of multiple fractures at different length scales. Because of their complexity at any given scale, they are particularly applicable to fragmentation and comminution [6] of homogeneous and heterogeneous materials, and a fractal fragment size distribution is expected [7].

Carpinteri [8] and Carpinteri et al. [9,10] used the fractal and multifractal approaches to explain the scaling laws for strength and toughness in the breaking behaviour of disordered materials.

Engleman et al. [11] applied the maximum entropy method to show that the number-size distribution follows a fractal law for fragments that are not too large. By combining a fractal analysis of brittle fracture with energy balance principles, in Refs. [12,13], a theoretical expression is derived for the fragment size distribution as a function of energy density. A fragment size distribution from clusters of connected bonds in a cubic lattice using percolation theory is predicted in Ref. [13]. A suite of fractal models has been developed [14–19]; these authors use the probabilities of failure to predict the fragment size distribution from the knowledge of the geometrical properties of the original material.

Recently, fragmentation has been studied from a physical [20], and geophysical point of view [21,22], for compression [23,24] and impact [25–28] as well as for comminution technologies [29,30].

Only more recently, a multifractal transition has been observed [31–33].

Relevant works in this area have been performed by Brown [34] that applied fractal scaling laws with limited success to coal powder comminution, and Mecholsky and Clupper [35] that identified fractals on fragments surfaces of highly brittle materials.

Fractal and fragmentation processes have been reviewed by Perfect [19]. A review on drilling indentation and the physical mechanisms of hard rock fragmentation under mechanical loading has been reported in Ref. [36].

The novelty of this paper is that the drilling comminution is theoretically and experimentally analyzed by a multifractal approach. According to some experiments on drilling detritus, a multifractal scaling law for the partial mass of fragments and its physical interpretation is consistently proposed. In addition, we show that the drilling strength (energy dissipated over volume removed) is strongly size-dependent and cannot be considered a material constant, as classically supposed. Consequently, a multifractal scaling law for the drilling strength is also proposed.

* Corresponding author. Tel.: +39-11-5644850; fax: +39-11-5644899.
E-mail addresses: carpinteri@polito.it (A. Carpinteri), pugno@polito.it (N. Pugno).
[1] Tel.: +39-11-5644902; fax: +39-11-5644899.

0032-5910/02/$ - see front matter © 2002 Elsevier Science B.V. All rights reserved.
doi:10.1016/S0032-5910(02)00335-2

2. Fractal energy dissipation and mass of fragments

After comminution or fragmentation, the *cumulative distribution* of particles with radius smaller than r can be assumed, as experimentally [7] and theoretically [11] suggested, of this form:

$$P(<r) = 1 - \left(\frac{r_{\min}}{r}\right)^D, \tag{1}$$

where experimentally it is $2<D<3$ and typically $D\cong 2.5$ [7]. The related boundary conditions are:

$$P(<r_{\min}) = 0, \tag{2a}$$

$$P(<r_{\max}) \cong 1, \tag{2b}$$

if $r_{\min} \ll r_{\max}$.

Of course, the complementary cumulative distribution of particles with radius larger than r is:

$$P(>r) = 1 - P(<r) = \left(\frac{r_{\min}}{r}\right)^D. \tag{3}$$

The *probability density function* $p(r)$ times the interval amplitude $\mathrm{d}r$ represents the percentage of particles with radius comprised between r and $r+\mathrm{d}r$. It is provided by derivation of the cumulative distribution function (1):

$$p(r) = \frac{\mathrm{d}P(<r)}{\mathrm{d}r} = D\frac{r_{\min}^D}{r^{D+1}}. \tag{4}$$

The total fracture surface area is obtained by integration:

$$A = \int_{r_{\min}}^{r_{\max}} N_{\mathrm{p}}(4\pi r^2)p(r)\mathrm{d}r, \tag{5}$$

where N_{p} is the total number of particles.

Introducing Eq. (4) into Eq. (5), we obtain ($2<D<3$):

$$\begin{aligned} A &= 4\pi N_{\mathrm{p}}\frac{D}{D-2}r_{\min}^D\left(\frac{1}{r_{\min}^{D-2}} - \frac{1}{r_{\max}^{D-2}}\right) \\ &\cong 4\pi N_{\mathrm{p}}\frac{D}{D-2}r_{\min}^2. \end{aligned} \tag{6}$$

On the other hand, the total volume of the particles is ($2<D<3$):

$$\begin{aligned} V &= \int_{r_{\min}}^{r_{\max}} N_{\mathrm{p}}\left(\frac{4}{3}\pi r^3\right)p(r)\mathrm{d}r \\ &= \frac{4}{3}\pi N_{\mathrm{p}}\frac{D}{3-D}r_{\min}^D(r_{\max}^{3-D} - r_{\min}^{3-D}) \\ &\cong \frac{4}{3}\pi N_{\mathrm{p}}\frac{D}{3-D}r_{\min}^D r_{\max}^{3-D}. \end{aligned} \tag{7}$$

One can assume a material "quantum" of size $r_{\min}=$ constant [21,36,37,42,43], and the hypothesis of self-similarity, i.e., $r_{\max} = \bar{k}\sqrt[3]{V}$, $\bar{k}=$constant [38,42]. The energy dissipated to produce the new free surface in the comminution process, which is provided by the product of fracture and friction energy Γ_{F} (for drilling $\Gamma_{\mathrm{F}}\cong 30\mathfrak{G}_{\mathrm{F}}$, being $\mathfrak{G}_{\mathrm{F}}$ the fracture energy, [42]) and total surface area $A/2$ (and not A the surface being in common between fragments) [39,40], is:

$$\begin{aligned} W &= \frac{1}{2}\Gamma_{\mathrm{F}}A = \mathfrak{G}_{\mathrm{F}}V\left(45\frac{3-D}{D-2}r_{\min}^{2-D}r_{\max}^{D-3}\right) \\ &= 45\frac{3-D}{D-2}\frac{\mathfrak{G}_{\mathrm{F}}}{r_{\min}^{D-2}\bar{k}^{3-D}}V^{D/3} = \mathfrak{G}_{\mathrm{F}}^{*}V^{D/3}, \end{aligned} \tag{8}$$

and represents an extension of the Third Comminution Theory, where $W\propto V^{2.5/3}$ [3].

The extreme cases contemplated by Eq. (8) are represented by $D=2$, surface theory [1,6], when the dissipation really occurs on a surface ($W\propto V^{2/3}$), and by $D=3$, volume theory [2,6], when the dissipation occurs in a volume ($W\propto V$). The experimental cases of comminution are usually intermediate ($D\cong 2.5$), as well as the size distribution for concrete aggregates due to Füller [41]. On the other hand, concrete aggregates frequently are a product of natural fragmentation or artificial comminution. If the material to be fragmented is concrete, we have therefore a double reason to expect $D\cong 2.5$.

The energy dissipation occurs on a two-dimensional surface according to Griffith [39], rather than on a morphologically fractal set. On the other hand, the distribution of particle size follows a power-law, the number of infinitesimal particles tending to infinity.

Usually, from comminution experiments [7], we get $2<D<3$, and only unfrequently values not belonging to such interval.

Eq. (7) can be utilized to compute the mass of the particles with radius smaller than r:

$$M(<r) \cong \frac{4}{3}\pi N_{\mathrm{p}}\rho_{\mathrm{m}}\frac{D}{3-D}r_{\min}^D r^{3-D}, \tag{9}$$

where $\rho_{\mathrm{m}}=$ material density, so that the ratio of this partial mass to the total mass is:

$$\frac{M(<r)}{M} \cong \left(\frac{r}{r_{\max}}\right)^{3-D}. \tag{10}$$

3. Material "quantum" and self-similarity assumptions

The fundamental assumptions of material "quantum" and of self-similarity can be derived from the more general hypothesis that the energy dissipation must occur in a fractal domain comprised, in any case, between a surface and a volume.

If we assume $D<2$, from Eq. (6), we have:

$$A \cong 4\pi N_{\mathrm{p}} \frac{D}{2-D} r_{\min}^{D} r_{\max}^{2-D}, \tag{11}$$

Eq. (7) is still valid and then Eq. (8) becomes:

$$W = \frac{1}{2}\Gamma_{\mathrm{F}} A = \frac{3}{2}\frac{3-D}{2-D}\frac{\Gamma_{\mathrm{F}}}{r_{\max}} V. \tag{12}$$

From Eq. (12), we obtain $r_{\max} = \bar{k}\sqrt[3]{V}$, if the dissipation is assumed to be proportional to $V^{2/3}$ even when $D<2$, i.e., $W \propto V^{2/3}$ if $D<2$.

If we assume $D>3$, from Eq. (7), we have:

$$V \cong \frac{4}{3}\pi N_{\mathrm{p}} \frac{D}{D-3} r_{\min}^{3}, \tag{13}$$

Eq. (6) is still valid and then Eq. (8) becomes:

$$W = \frac{1}{2}\Gamma_{\mathrm{F}} A = \frac{3}{2}\frac{D-3}{D-2}\frac{\Gamma_{\mathrm{F}}}{r_{\min}} V. \tag{14}$$

From Eq. (14), we obtain $r_{\min}$ = constant, if the dissipation is assumed to be proportional to V even when $D>3$, i.e., $W \propto V$ if $D>3$.

So, we have extended Eq. (8) for fractal exponent lower than 2 and larger than 3 ($W \propto V^{2/3}$ if $D<2$ and $W \propto V$ if $D>3$). In addition, we have shown that the self-similar hypothesis and the assumption of a material quantum are in a bijection correspondence with an energy dissipation comprised in any case between a surface or a volume.

4. Multifractal approach

A simple model, based on the concept of renormalization, illustrates how self-similar fragmentation can result in a (mono-) fractal size distribution [7].

If a cube, in a recursive process, is fragmented at each step with probability f into eight cubes (of 1/2 linear dimension), the volume of one fragment and the number of fragments (cubes) at the n-th step will be:

$$V_n = \frac{1}{8^n} V_0, \tag{15}$$

$$N_n = (8f)^n N_0, \tag{16}$$

where V_0 is the volume of the N_0 original cubes. Taking the natural logarithms of both Eqs. (15) and (16) and eliminating n from them gives:

$$\frac{N_n}{N_0} = \left(\frac{V_n}{V_0}\right)^{-\frac{\ln 8f}{\ln 8}}. \tag{17}$$

If a fragmented cube produces at each step, a generic integer number V_0/V_1 of cubes, noting that $V_n = 4/3\pi r_n^3$, Eq. (17) can be generalized as:

$$\frac{N_n}{N_0} = \left(\frac{r_n}{r_0}\right)^{-3\frac{\ln\frac{V_0}{V_1} f}{\ln\frac{V_0}{V_1}}}. \tag{18}$$

From the comparison with the well-known definition of fractal set:

$$N_n = \frac{C}{r_n^D}, \tag{19}$$

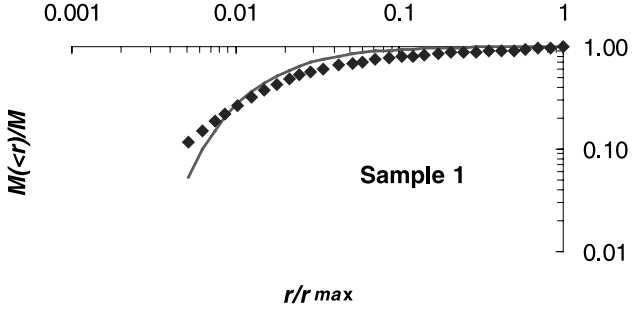

Fig. 1. Relative size vs. relative mass of fragments. Comparison between theoretical multifractal approach of Eq. (25) (with $r_{\min}$ = 0.5 μm and $r_{\max}$ = 175 μm) and experimental points for Sample 1 (for which $r_{\max}$ = 175 μm and $r_{\min}$ = 0.9 μm).

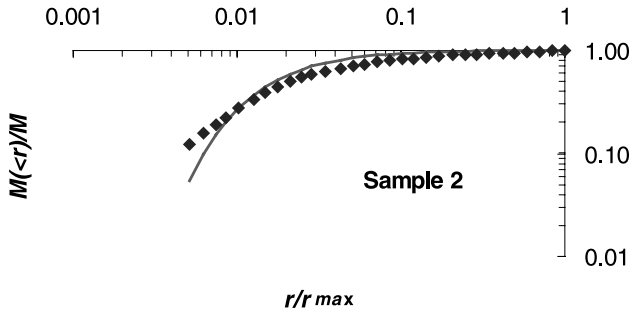

Fig. 2. Relative size vs. relative mass of fragments. Comparison between theoretical multifractal approach of Eq. (25) (with $r_{\min}$ = 0.5 μm and $r_{\max}$ = 175 μm) and experimental points for Sample 2 (for which $r_{\max}$ = 175 μm and $r_{\min}$ = 0.9 μm).

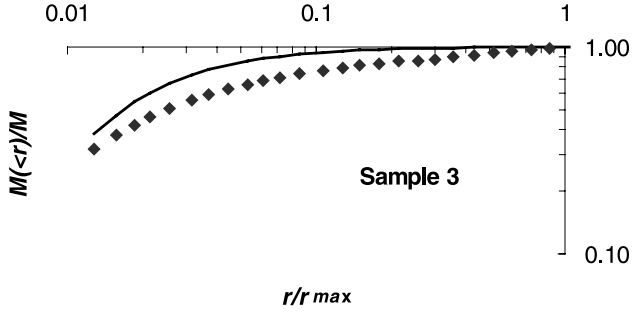

Fig. 3. Relative size vs. relative mass of fragments. Comparison between theoretical multifractal approach of Eq. (25) (with $r_{\min}$ = 0.5 μm and $r_{\max}$ = 175 μm) and experimental points for Sample 3 (for which $r_{\max}$ = 182.5 μm and $r_{\min}$ = 2.25 μm).

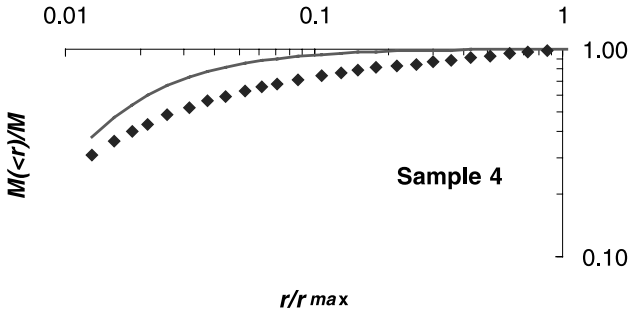

Fig. 4. Relative size vs. relative mass of fragments. Comparison between theoretical multifractal approach of Eq. (25) (with $r_{min}=0.5$ μm and $r_{max}=175$ μm) and experimental points for Sample 4 (for which $r_{max}=182.5$ μm and $r_{min}=2.25$ μm).

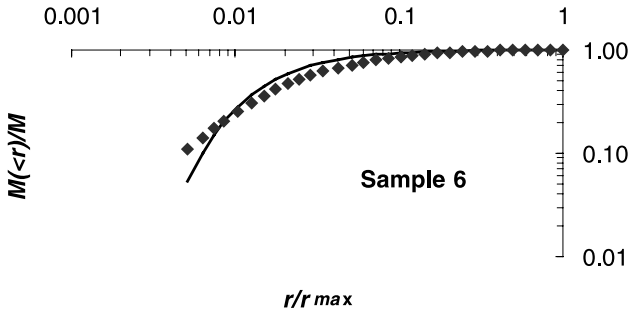

Fig. 6. Relative size vs. relative mass of fragments. Comparison between theoretical multifractal approach of Eq. (25) (with $r_{min}=0.5$ μm and $r_{max}=175$ μm) and experimental points for Sample 6 (for which $r_{max}=103$ μm and $r_{min}=0.9$ μm).

we obtain:

$$D = 3\frac{\ln\frac{V_0}{V_1}f}{\ln\frac{V_0}{V_1}}. \tag{20}$$

From Eq. (20), we deduce the probability of fragmentation f (in any case greater than V_1/V_0):

$$f = \left(\frac{r_1}{r_0}\right)^{3-D}. \tag{21}$$

In other words, assuming a constant probability of fragmentation f, we can describe a self-similar process and obtain a constant fractal exponent D. In spite of this, the "quantum" material existence implies that the phenomenon must change when the fragment dimension approaches the dimension of the unbreakable material "quantum". The probability of fragmentation should increase with fragment size and the corresponding exponent D should also increase according to Eq. (20). A non-constant exponent D in Eq. (19) permits to describe a multifractal law [8]. The rupture of self-similarity in the fragmentation process should be due to the existence of the material "quantum" and represents the physical reason of the multifractal character.

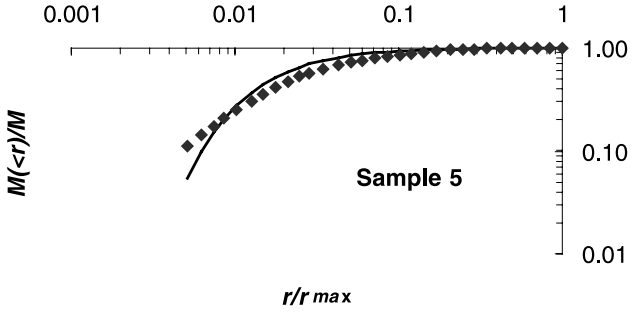

Fig. 5. Relative size vs. relative mass of fragments. Comparison between theoretical multifractal approach of Eq. (25) (with $r_{min}=0.5$ μm and $r_{max}=175$ μm) and experimental points for Sample 5 (for which $r_{max}=123$ μm and $r_{min}=0.9$ μm).

Some experiments on conventional drilling perforation (on conventional concrete ($\sigma_u=30$ MPa, $\mathfrak{G}_F=100$ N/m), [42]) have been performed. The results obtained for the drilling detritus are reported (experimental points) in Figs. 1–6. According to Eq. (10), the slope of the curves reported in Figs. 1–6 is equal to $3-D$, so that experimentally we have:

$$D_{min} = D(r=r_{min}) \cong 2, \quad D_{max} = D(r=r_{max}) \cong 3, \tag{22}$$

as well as the corresponding probabilities are (see Eq. (21)):

$$f_{min} = f(r=r_{min}) = \frac{r_1}{r_0}, \quad f_{max} = f(r=r_{max}) = 1. \tag{23}$$

According to these considerations, the following very simple variation of the multifractal exponent D can be proposed:

$$D(r) = 3 - \frac{r_{min}}{r}. \tag{24}$$

5. Scaling laws for drilling detritus and drilling strength. A comparison between theory and experiments

As a consequence of Eq. (24), the fractal law (10) may be consistently rewritten as multifractal (Fig. 2):

$$\frac{M(<r)}{M} \cong \left(\frac{r}{r_{max}}\right)^{\frac{r_{min}}{r}}. \tag{25}$$

The multifractal scaling law (25) can be used to a description of the experimental results obtained from drilling comminution (Fig. 7). The experiments have been performed by a laser diffraction sensor HELOS. This system is the first for which the Fraunhofer method is applied over the whole measuring range from 0.1 to 8750 μm. It is the classical instrument for dry and wet particle size analysis of powders, suspensions, emulsions or sprays.

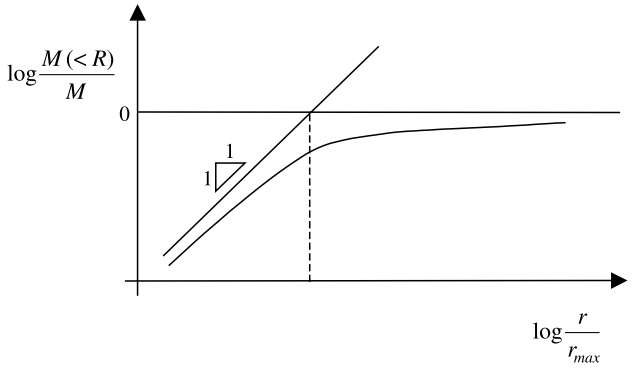

Fig. 7. Multifractal scaling law for relative mass vs. relative size of fragments.

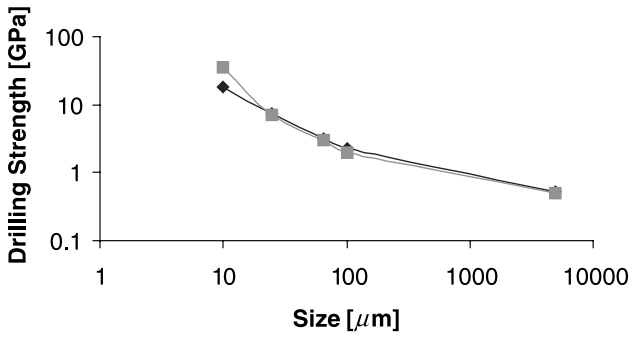

Fig. 9. Scaling law for drilling strength vs. size-scale. Experimental results (squares) and theoretical points (rhombs) from Eq. (28) with $l_{ch} = 2r_{max} \approx 350$ μm and $S_\infty = 0.5$ GPa.

From these experiments, the characteristic size of the material "quantum" appears to be approximately equal to $r_{min} \cong 0.5$ μm. It is interesting to note that this value is far from the size measurement accuracy (0.05 μm).

Theoretical predictions (Eq. (25)) are reported (continuous curves) in Figs. 1–6. It is interesting to emphasize that the multifractal scaling law presented in these Figs. 1–6 is not a best fit. For this reason, some discrepancies can be found. This curve is the same for all Figs. 1–6 and it coincides with Eq. (25) in which we suppose $r_{max} = 175$ μm and $r_{min} = 0.5$ μm. Nevertheless, we observe for Samples 1, 2, 5, 6 a good quantitative agreement. For Samples 3 and 4, the agreement is rather poor. The physical reason is that the corresponding drilling processes have been performed with modified segments to reduce the comminution and optimize the cutting ability of the tool.

Classically, the drilling strength (energy dissipated over volume removed) is considered a size-independent parameter. On the other hand, experiments show that it could be variable with size (especially at small scale) by several orders of magnitude! In a bilogarithmic diagram of drilling strength versus size-scale (of the volume drilled per unit time), a dimensional transition of the "fractal drilling strength" $\mathfrak{G}_F^*$ of Eq. (8) from a substantial fracture energy (energy/surface) for smaller sizes to a substantial compressive strength (energy/volume) for larger sizes can be described.

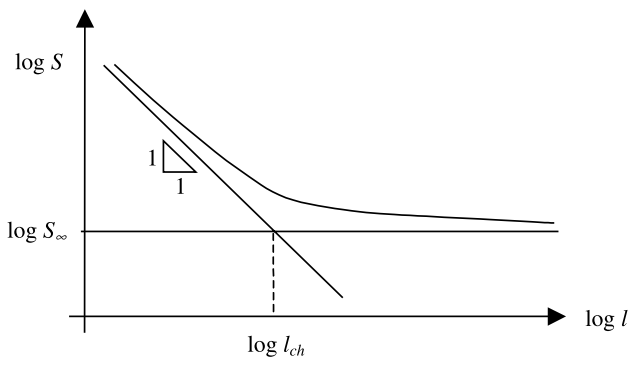

Fig. 8. Multifractal scaling law for drilling strength vs. size-scale.

From Eq. (8), we have in fact:

$$S = \frac{W}{V} = \mathfrak{G}_F^* l^{D-3}, \tag{26}$$

if $V = l^3$ is the volume drilled per unit time, and therefore:

$$\log S = \log \mathfrak{G}_F^* + (D-3)\log l. \tag{27}$$

The slope of the slanted asymptote is equal to minus one (-1), so that the nominal drilling strength $S = W/V$ decreases with size l.

If $D = 2$, the slope is -1, as well as $D = 3$ implies a vanishing slope.

According to these considerations, the following multifractal scaling law for drilling strength (Fig. 8) can be proposed:

$$S = S_\infty \left(1 + \frac{l_{ch}}{l}\right), \tag{28}$$

where the two material constants S_∞ and l_{ch} can be experimentally obtained. S_∞ is the drilling strength for very large scale and l_{ch} is a characteristic length of the order of the size of the largest fragment, modelling the transition between the two regimes shown in Fig. 8. An experimental curve for the size effect on drilling strength, obtained from single scratch tests [42], is reported in Fig. 9. As theoretically deduced, the size effect on nominal drilling strength appears very clearly.

6. Conclusions

The drilling comminution has been theoretically and experimentally analyzed by a multifractal approach. The proposed theory emphasizes how the energy dissipation in

the comminution process occurs in a fractal domain comprised between a surface and a volume (Eq. (8)) with size-dependent multifractal exponent D, ranging from 2 for small sizes, to 3 for large sizes.

The transitional multifractal exponent of the fragment size distribution has been experimentally observed (Figs. 1–6). According to these considerations, very simple multifractal scaling laws for the drilling detritus (Eq. (25)) have been consistently proposed.

Classically, the drilling strength (energy dissipated over volume removed) is considered a size-independent parameter. On the other hand, experiments (Fig. 9) show that it could be variable with size (especially at small scale) by several orders of magnitude! According to these considerations, the multifractal scaling law of Eq. (28) for drilling strength has been also proposed.

The theoretical assumption of a material "quantum" has been experimentally observed and its characteristic dimension (diameter) appears, for the drilled concrete, to be close to 1 μm.

7. Notation

Greek letters

ρ_m	material density
$\mathfrak{G}_F$	fracture energy
Γ_F	fracture and friction energy
$\mathfrak{G}_F^*$	fractal fracture and friction energy or fractal drilling strength

Latin letters

A	total fracture surface area of fragments
D	fractal exponent
f	probability of fragmentation
l	characteristic length of the fragmented volume
l_{ch}	internal characteristic length of the material
N	number of fragments
M	total mass of fragments
$M(<r)$	mass of fragments with radius smaller than r
p	probability size-distribution function for fragments
P	cumulative size-distribution function for fragments
r	fragment size
r_{max}	size of the largest fragment
r_{min}	size of the smallest fragment (material quantum)
S	drilling strength
S_∞	drilling strength for infinite size
V	fragmented volume
W	energy dissipated during fragmentation

Acknowledgements

The present research was carried out with the financial support of Ministry of University and Scientific Research (MURST), National Research Council (CNR) and EC-TMR Contract N° ERBFMRXCT960062.

References

[1] P.R. Rittinger, Lehrbuch der Aufbereitungskunde, Berlin, 1867.
[2] F. Kick, Das Gesetz der Proportionalen Widerstände, Leipzig, 1885.
[3] F.C. Bond, Min. Eng. 4 (1952) 484 (Aime Trans. 193).
[4] B.B. Mandelbrot, The Fractal Geometry of Nature, Freeman, New York, 1982.
[5] J. Feder, Fractals, Plenum, New York, 1988.
[6] D. Béla Beke, Principles of Comminution, Publishing House of the Hungarian Academy of Sciences, Budapest, 1964, pp. 90–92.
[7] D.L. Turcotte, Fractals and Chaos in Geology and Geophysics, Cambridge Univ. Press, Cambridge, 1992, pp. 20–32.
[8] A. Carpinteri, Int. J. Solids Struct. 31 (1994) 291.
[9] A. Carpinteri, B. Chiaia, Chaos, Solitons Fractals 8 (1997) 135.
[10] A. Carpinteri, G. Ferro, I. Monetto, Mag. Concr. Res. 51 (1999) 217.
[11] R. Engleman, N. Rivier, Z. Jaeger, J. Appl. Phys. 63 (1988) 4766.
[12] Z. Yong, M.T. Hanson, Chaos, Solitons Fractals 7 (1996) 31.
[13] A. Aharony, A. Levi, R. Englman, Z. Jaeger, Ann. Isr. Phys. Soc. 8 (1986) 112.
[14] M. Matsushita, J. Phys. Soc. Jpn. 54 (1985) 857.
[15] D.L. Turcotte, J. Geophys. Res. 91 (1986) 1921.
[16] D.L. Turcotte, Pure Appl. Geophys. 131 (1989) 171.
[17] M. Rieu, G. Sposito, Soil Sci. Soc. Am. J. 55 (1991) 1231.
[18] J.W. Crawford, B.D. Sleeman, J.M. Young, J. Soil Sci. 44 (1993) 555.
[19] E. Perfect, Eng. Geol. 48 (1997) 185.
[20] E. Ben-Naim, P.L. Krapivsky, Phys. Lett., A 275 (2000) 48.
[21] C.G. Sammis, Fractal fragmentation and frictional stability in granular materials, IUTAM Symposium on Mechanics of Granular and Porous Materials, Kluwer Academic Publishing, The Netherlands, 1997, pp. 23–34.
[22] P. Hyslip, L.E. Vallejo, Eng. Geol. 48 (1997) 231.
[23] A.W. Momber, Eng. Fract. Mech. 67 (2000) 445.
[24] D. Schocke, H. Arastoopour, B. Bernstein, Powder Technol. 102 (1999) 207.
[25] A.D. Salman, D.A. Gorham, Powder Technol. 107 (2000) 179.
[26] G. Belingardi, A. Gugliotta, A. Vadori, Int. J. Impact Eng. 21 (1998) 335.
[27] E.S.C. Ching, S.L. Lui, K.-Q. Xia, Physica, A 287 (2000) 83.
[28] J. Tomas, M. Schreier, T. Gröger, S. Ehlers, Powder Technol. 105 (1999) 39.
[29] I. Larsson, H.G. Kristensen, Powder Technol. 107 (2000) 175–178.
[30] P. Cleary, Int. J. Numer. Anal. Methods Geomech. 25 (2001) 83.
[31] O. Sotolongo-Costa, A.H. Rodriguez, G.J. Rodgers, Physica, A 286 (2000) 638.
[32] E.S.C. Ching, Physica, A 288 (2000) 402.
[33] C.A. Hecht, Pure Appl. Geophys. 157 (2000) 487.
[34] G.J. Brown, Miner. Eng. 10 (1997) 229.
[35] J.J. Mecholsky, D.C. Clupper, 3rd World Congress on Particle Technology, IchemE, Brigthon, Paper 127.
[36] L.L. Mishnaevsky, Int. J. Rock Mech. Min. Sci. Geomech. Abstr. 32 (1995) 763.
[37] V. Novozhilov, Prikl. Mat. Meh. 33 (1969) 212.
[38] A. Carpinteri, Mechanical Damage and Crack Growth in Concrete, Martinus Nijhoff, Dordrecht, The Netherlands, 1986.
[39] A.A. Griffith, Philos. Trans. R. Soc. Lond., A 221 (1921) 163.
[40] A. Smekal, Physikalisches und Technisches Arbeitsgesetz der Zerkleinerung, Zeitschr. VDI, Beiheft Verfahrenstechnik, 1937, pp. 159–161.
[41] P. Stroeven, International Symposium on Brittle Matrix Composites III, Warsaw, Poland, 1991, pp. 1–10.
[42] A. Carpinteri, N. Pugno, Numer. Anal. Methods Geomech. 26 (2002) 499.
[43] K. Kendall, Nature 272 (1978) 711.